Predicted strong spin-phonon interactions in Li-doped diamond

Francesco S. Gentile [1], William C. Mackrodt [1,2], Neil L. Allan [2] and Roberto Dovesi [1]

1. *Dipartimento di Chimica, Università di Torino,Via P.Giuria 5, 10125 Torino, Italy*
2. *School of Chemistry, University of Bristol, Cantock's Close, Bristol BS8 1TS, England*

Abstract

DFT calculations of the Li substitutional defect in diamond based on the B3LYP functional and a 64-atom supercell indicate that (i) the quartet (S_z=3/2) state is lower in energy than the doublet (S_z=1/2) state by 0.07 eV (810 K) for fully relaxed static structures and by 0.09 eV (1045 K) with the inclusion of zero-point vibrations, (ii) the effective charges at the Li and four neighbouring C sites is similar in the two spin states, but there are substantial differences in the corresponding spin distributions, and (iii) there are unprecedented differences in the Raman spectra of the two spin states, in terms of both frequency distributions and intensities, that can most reasonably be attributed to strong spin-phonon coupling, in view of the very similar charge distributions in the two states. These differences are an order of magnitude greater than those reported previously for any bulk transition metal or rare-earth compound. The basis sets and functional used in these calculations predict many of the relevant constants (a_0, c_{11}, c_{44}) of diamond mostly to within 1% of the experimental values, most notably the TO(X) Raman frequency and the phonon density of states. Comparisons with the calculated Raman spectra of the quintet (S_z=2) and singlet (S_z=0) spin states of the neutral vacancy defect, which have similar spin distributions at the four neighbouring C atoms (C_n) to the vacancy site as those at the corresponding C_n sites in the quartet and singlet states of the Li defect, show that the differences in the two Raman spectra of the latter defect are closely related to those in the former.

Introduction

The properties of impurity defects in diamond have been investigated for many years, leading to a wide range of applications from high temperature thermistors[1] to synchrotron beam monitors,[2] and, most recently quantum dots,[3,4] with many of these reliant on the result of previous theoretical and computational studies .[5,6,7,8,9,10] This Edge reports new, and quite unexpected properties that are predicted for

one such impurity, namely, Li, and are related to the unprecedent coupling of its unpaired spin and the local and collective lattice vibrations. While there are previous accounts of some aspects of the electronic structure of Li-doped diamond,[11,12,13,14] there are no reports of the vibrational properties, including the specific new features we report here.

Spin-lattice interactions such as magnetostriction and spin-lattice relaxation, are well known in spectroscopy, with numerous recent reports of spin-phonon coupling in the Raman spectra of several systems.[15,16,17,18,19,20] Four characteristic features of these accounts are that (i) they frequently involve spin states with differences (spin gap) of the order of meV (10 K), and hence are effective at low temperature, (ii) the differences in the spectra are small, typically a few cm $^{-1}$, (iii) they refer to periodic magnetism, at least within Individual domains, where collective effects are important, and (iv) they appear to be confined to systems containing transition metal or rare-earth components. More recently, Webster *et al.*[21] reported the calculated Raman spectra of 2-dimensional ferromagnetic (FM) and antiferromagnetic (AFM) CrI_3, where difference in energy between the two spin states was found to be 150 - 160 K with shifts in frequency of up to 10 cm^{-1}, although the spectral profiles are much the same. However, it is not clear as to whether these differences are intrinsic to CrI_3, or the result of the reduced dimensionality. This Edge reports predicted strong spin-phonon coupling in a radically new system containing no transition metal or rare-earth element. It is Li-doped diamond, for which (i) the gap in energy between the two possible spin states is ~800 K, which is at least an order of magnitude greater than the majority of previous reports, (ii) the profiles of the Raman spectra of the two spin states are radically different, with shifts in both the frequencies and intensities that are, again, an order of magnitude greater than previous reports and (iii) the interactions are local, rather than periodic, and hence have no cooperative component. They derive from all-electron calculations based the B3LYP approximation to DFT, based on Gaussian orbitals and formulated within a periodic supercell approach to local lattice defects, as implemented in the CRYSTAL17 programme.[22]

Computational Methods

For the most part, our calculations utilize the B3LYP global hybrid functional,[23,24] as implemented in the CRYSTAL program.[25] Pople's standard 6-21G[26] *all-electron* basis sets of Gaussian type functions were adopted for carbon, re-optimizing the exponent of the outermost *sp* orbitals (0.23 Bohr^{-2}) in bulk diamond. For the lithium dopant the triple-ζ basis set Li_pob_TZVP (https://www.crystal.unito.it/Basis_Sets/lithium.html)[27] was used in order to obtain an accurate description of the Li-C interaction. Truncation of the Coulomb and exchange infinite lattice series was controlled by five thresholds, T_i , which were set to 7 (T_1 -T_3), 9 (T_4) and 30 (T_5). The convergence threshold on the energy for the self-consistent-field (SCF) procedure was set to $10^{-8}E_h$ for structural optimizations and to 10^{-11} E_h for vibrational frequency calculations. The DFT exchange-correlation contribution and its gradient were evaluated by numerical integration over the unit cell volume. The generation of the integration grid points was based on an atomic partition method, originally proposed by Becke,[28] in which

the radial and angular points are obtained from a Gauss-Legendre quadrature and the Lebedev two-dimensional distributions respectively. The choice of a suitable grid is crucial both for numerical accuracy and cost consideration. In this study a pruned grid with 75 radial and 974 angular points was used. Reciprocal space sampling was based on a regular Pack-Monkhorst[29] sub-lattice grid centred at the Γ point (*i.e.* at the centre of the first Brillouin zone), leading to 4 sample points, along each of the reciprocal lattice vectors. This corresponds to 13 **k**-points in the irreducible part of the Brillouin zone after point symmetry has been taken into account.

A Supplementary Material Section contains some of the technical details concerning the calculation of the vibrational spectra.

Results and Discussion

Here 64-atom supercells have been used, which previous reports have shown to be suitable for the calculation of vibrational spectra of defective systems, providing convergent data compared with supercells of 128, 216, 512 and 1000 atoms.[30,31,32] An essential prelude to defect calculations is a check on the accuracy with which the computational methodology, here the basis sets and choice of functional, describes the relevant features of the (perfect) host lattice.

Table I

Calculated properties of the diamond lattice based on the present C basis set and B3LYP functional. a_0 (Å) is the lattice parameter, c_{11} and c_{44} (10^{12} dyn cm^{-2}) are elastic constants, ε is the high frequency dielectric constant and ν_{TO} (Γ) (cm $^{-1}$) is the Raman vibrational mode at the centre of the first Brillouin zone (Γ point).

Property	Calculated	Observed
a_0	3.603 (1%)	3.567 [33]
c_{11}	10.68 (1%)	10.79 [34]
c_{44}	5.76 (0.3%)	5.78 [34]
ε	5.43 (5%)	5.7[35]
ν_{TO} (Γ)	1317 (1%)	1332 [36]

As Table I indicates, the predicted lattice constant, a_0, c_{11} and c_{44} elastic constants and most significantly, the Raman frequency, $\nu_{TO(X)}$, are mostly to within 1% of the experimental values, while Figure 1 shows that the calculated phonon density of states (DOS) is in excellent agreement with that obtained from inelastic X-Ray scattering,[37] so that it is reasonable to expect comparable accuracy for predictions for the defective lattice.

In principle there are two modes of Li solution in diamond, interstitial, where there are two high symmetry sites, tetrahedral and hexagonal, and substitutional, for which there are three possible spin states. This letter is concerned solely with substitutional Li, which is predicted to be the more stable of the two modes by over 1 eV. The three spin states of the substitutional mode arise from the combined spins of Li and the four unpaired spins on the neighbouring C atoms, leading states with S_z = 5/2, 3/2 and 1/2. The sextet is found to be unstable, leaving the quartet

(3/2) and doublet (1/2) as the two possible ground states of the system. Since Li substitution in diamond can also be viewed as a Li interstitial at a vacancy site, it might be insightful to compare some of the properties of the substitutional Li defect with those of the diamond vacancy.

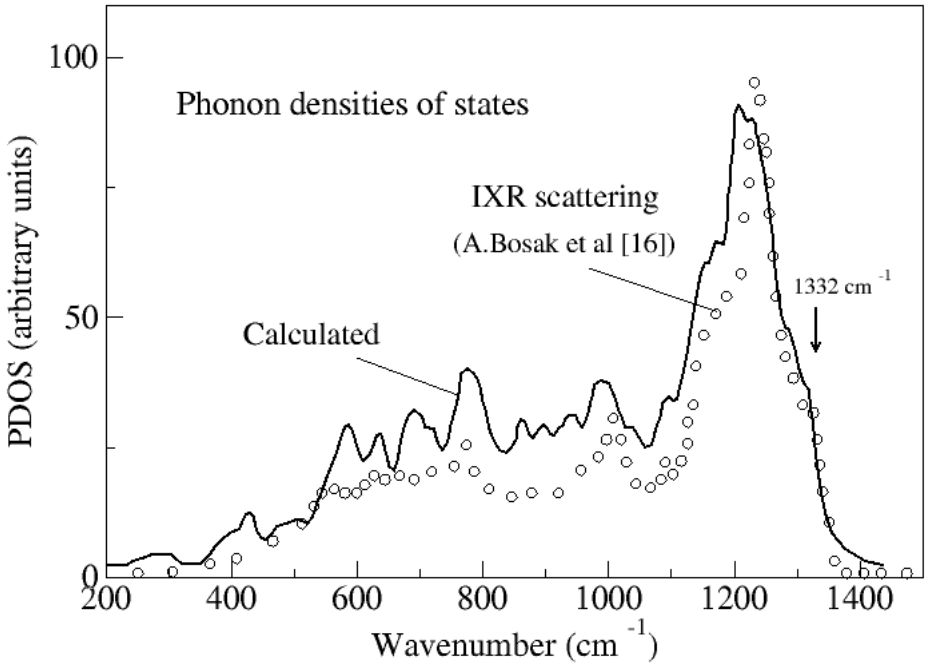

Figure 1

Comparison of the calculated phonon densities of states with the IXR scattering data reported by Bosak *et al*[37]

Table II

Predicted energies (eV/cell) and thermodynamic functions (T = 298.15 K, P = 0.10132500 MPa) of $(C_{63}Li)_{3/2}$ and $(C_{63}Li)_{1/2}$, where E_u and E_L are the unrelaxed and relaxed lattice energies, E_r, the relaxation energy, E_0, the zero-point energy, E_T, the thermal contribution to the vibrational energy and S the entropy.

Energy	$(C_{63}Li)_{3/2}$	$(C_{63}Li)_{1/2}$	Δ(3/2 - 1/2)
E_u	-65432.5584	-65432.2180	-0.3403
E_L	-65436.3754	-65436.3087	-0.0667
E_r	-3.8170	-4.0907	+0.2737
E_0	11.2982	11.3034	-0.0052
E_T	0.3497	0.3410	0.0087
S (meV/(cell.K))	1.5962	1.5229	+0.0733
E_T+PV-TS	-0.1259	-0.1129	-0.0130
$E_L+E_0+E_T$+PV-TS	-65425.2031	-65425.1182	-0.0849

Starting with the relative stabilities, Table II lists the calculated energies of fully relaxed (structural and dynamic) 64 atom supercells of the two spin states, referred to as $(C_{63}Li)_{3/2}$ and $(C_{63}Li)_{1/2}$, where lattice relaxation energies, E_r, of 3.82 eV and 4.09 eV respectively are close to 70% of the optical gap of 5.7 eV. The calculated difference in energy between the two states varies from 0.34 eV (3950 K) for the

unrelaxed lattices and 0.07 eV (810 K) for the relaxed structures, to 0.09 eV (1045 K) for the difference in free energy, including vibrational contributions. Thus, the difference in the zero-point vibration contributions increases the stability of the 3/2 state by 0.02 eV (235 K). Details of the corresponding fully relaxed lattice structures of $(C_{63}Li)_{3/2}$ and $(C_{63}Li)_{1/2}$ are given in Table III.

Table III

Comparison of the Li-C_n and Li-C_{nn} (nearest and next nearest neighbour) bond lengths (Å) in the fully relaxed structures of $(C_{63}Li)_{3/2}$ and $(C_{63}Li)_{1/2}$, where δ are the percentage differences from those in the perfect lattice. The number of neighbours at a given distance are in parentheses. There are four first neighbours and twelve second neighbours. Their distances from the reference atom are the same in perfect diamond and split into subsets after relaxation.

Bond lengths	C	$(C_{63}Li)_{3/2}$	$\delta_{3/2}$	$(C_{63}Li)_{1/2}$	$\delta_{1/2}$
(Li-C_n)(4)	1.560	1.790(1) 1.792(3)	0.230(14%) 0.232(14%)	1.7323(1) 1.8139(2) 1.8141(1)	0.1723(11%) 0.1723(11%) 0.2541(15%)
(Li-C_{nn})(12)	2.547	2.571(3) 2.574(6) 2.578(3)	0.024(1%) 0.027(1%) 0.031(1%)	2.464(3) 2.569(6) 2.7033(3)	0.083(3%) 0.022(1%) 0.1563(6%)

This shows that the changes in the two lattices in the immediate vicinity of the Li substituent are close, if not identical, with increases of 14% in the two non-equivalent Li-C_n distances in $(C_{63}Li)_{3/2}$, as opposed to increases of 11% and 15% in the corresponding distances in $(C_{63}Li)_{1/2}$. The changes in Li-C_{nn}, the next neighbour separations, are an order of magnitude smaller, at ~1%, so that, overall, the structures of the two defective lattices are very similar.

Table IV

Band gaps, atomic net charges, q (|e|), and magnetic moments (atomic spin densities), s (|e|), as obtained from a Mulliken partition of charge and spin densities, at Li, C_n and C_{nn} sites in $(C_{63}Li)_{3/2}$ and $(C_{63}Li)_{1/2}$. The number of neighbours at the same distance is indicated in parentheses. Σ_4 C_n and Σ_{12} C_{nn} are the sum of the charges over the four first or twelve second neighbours, respectively, of the quantities in the column indicated. α and β superscripts indicate the spin. The Δ columns give the differences between the two spin states.

	$(C_{63}Li)_{3/2}$				$(C_{63}Li)_{1/2}$				Δ			
	unrelaxed		Relaxed		unrelaxed		relaxed		unrelaxed		relaxed	
E_g	5.53$^{\alpha}$, 1.48$^{\beta}$		5.26$^{\alpha}$, 1.41$^{\beta}$		0.74$^{\alpha}$, 0.43$^{\beta}$		1.63$^{\alpha}$, 1.55$^{\beta}$		-4.79$^{\alpha}$, -1.05$^{\beta}$		-3.63$^{\alpha}$, -0.14$^{\beta}$	
Sites	**q**	**s**	**q**	**S**	**q**	**s**	**q**	**s**	**Q**	**s**	**q**	**s**
Li	0.35	0.30$^{\alpha}$	0.28	0.25$^{\alpha}$	0.34	0.10$^{\alpha}$	0.27	0.07$^{\alpha}$	0.01	0.20$^{\alpha}$	0.01	0.18$^{\alpha}$
C_n	-0.09(4)	0.56$^{\alpha}$(4)	-0.07(1) -0.07(3)	0.62$^{\alpha}$(1) 0.62$^{\alpha}$(3)	-0.10(2) -0.07(2)	0.32$^{\beta}$(2) 0.69$^{\alpha}$(2)	-0.09(1) -0.05(2) -0.05(1)	0.79$^{\beta}$(1) 0.55$^{\alpha}$(2) 0.55$^{\alpha}$(1)	- -	- -	- -	- -
Σ_4 C_n	-0.36	2.24$^{\alpha}$	-0.28	2.46$^{\alpha}$	-0.35	0.74$^{\alpha}$	-0.24	0.86$^{\alpha}$	-0.01	1.50$^{\alpha}$	-0.04	1.60$^{\alpha}$
Σ_{12} C_{nn}	0.04	0.16$^{\beta}$	-0.08	0.47$^{\beta}$	0.03	0.01$^{\alpha}$	-0.05	0.00$^{\alpha}$	0.01	0.60$^{\alpha}$	0.03	0.23$^{\alpha}$

Turning now to the electronic structures, and, in particular, to the charge and spin distributions, Table IV lists these for both the unrelaxed and relaxed structures of the two spin states, from which a number of important points emerge. The first is that in both the unrelaxed and relaxed structures, the (Mulliken) charges at the Li, C_n and C_{nn} sites are all very close in $(C_{63}Li)_{3/2}$ and $(C_{63}Li)_{1/2}$, with differences of 0.02 (|e|), or less. It follows from this that the electrostatic contributions to the

lattice potential in the two spin states are similar. By virtue of the difference in overall spin between the two states, $\Delta S=1$, the *magnitudes* of the spins at individual lattice sites (again evaluated through a Mulliken partition of the total spin) in the two states might reasonably be expected to differ, by roughly a factor of three. However, as Table IV shows clearly this is not the case in a number of respects. In $(C_{63}Li)_{3/2}$ the spins are all aligned, with 8% of the total spin at Li, 82% at C_n, and 10% at C_{nn} and subsequent neighbours in the relaxed structure, with a similar, though not exact, distribution in the unrelaxed lattice. In $(C_{63}Li)_{1/2}$, on the other hand, while the distribution of total spin is broadly the same, with 7% of the total spin at Li, 86% at C_n, and 7% at C_{nn} and subsequent neighbours in the relaxed structure, the C_n sites contain both α and β spins. Again, in the unrelaxed lattice, the broad distribution of total spin is similar, but with a re-arrangement of α and β spins at the C_n sites. These can be compared with the charge and spin distributions at the vacancy sites where there is minimal ($\leq$ -0.05 |e|) density at V, and re-distributions of charge from the C_n to the C_{nn} sites, leaving the former with charges of +0.12 |e|, +0.17 |e| and +0.19 |e| spins of 0 ($2\times0.71^{\alpha}$, $2\times0.71^{\beta}$), 1.89 |e| ($3\times0.77^{\alpha}$, 0.42^{β}) and 2.00 |e| in the singlet, triplet and quintet states respectively.

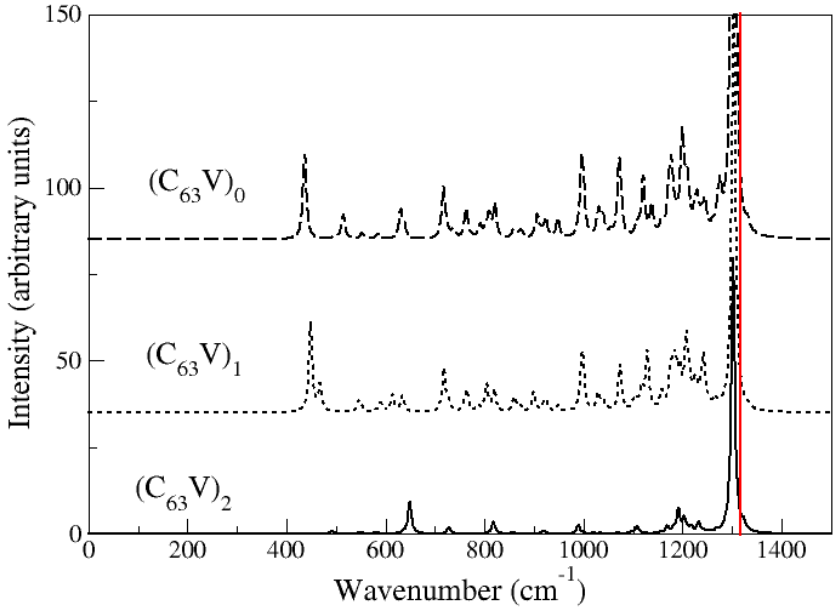

Figure 2.
Calculated Raman spectra of the singlet, $(C_{63}V)_0$, triplet, $(C_{63}V)_1$, and quintet, $(C_{63}V)_5$, states of the vacancy (off set). The 1318 cm $^{-1}$ ($\nu_{TO(X)}$) diamond line is shown in red.

Of less direct importance in the present context, though still of interest with regard to the electrical properties of Li: diamond, Table IV reveals that in the unrelaxed lattice, the doublet state state is a stronger acceptor than the quartet by roughly a factor of 2; and that while lattice relaxation has little effect on the latter, it roughly doubles the gap of the doublet state, so that the two states have acceptor states

which differ in energy by less than 0.3 eV. Again, these differ from the vacancy gaps, where there are relatively minor differences between the two spin states, although the acceptor levels in $(C_{63}V)_0$ and $(C_{63}Li)_{3/2}$ are similar at ~1.5 eV, which might be a source of confusion.

Turning now to the central results of this Edge, since the host lattice has a *single* Raman absorption, namely, the first order scattering of triply degenerate TO(X) phonons of t_{2g} symmetry at 1332 cm^{-1} (the present calculations predict a value of 1318 cm^{-1} (-1% from experiment)), *all* absorptions at other frequencies must involve either V or Li, or both, to a greater or lesser extent. Starting with the vacancy spectra, Figure 2 shows that the calculated Raman spectra of the three spin states of the diamond vacancy all retain the host TO(X) line, albeit blue-shifted by 20 cm^{-1} (1.5%). However, elsewhere in the spectra there are two important differences between the singlet and triplet spectra, on the one hand, and the quintet. The first is that the former contains a moderately strong absorption in the region of 400 cm^{-1}, whereas the quintet spectrum is essentially null here; the second is that the region, 600 cm $^{-1}$ to 1100 cm $^{-1}$, which contains the collective modes, is substantially richer and stronger in the singlet and triplet spectra than the quintet. It is evident that even for the vacancy, which might be considered as a precursor for Li substitutional defects, strong spin-phonon coupling occurs, with a clear distinction between the quintet state, with an all parallel {αααα} spin arrangement of the C_n atoms, and the singlet and triplet states, where the C_n atoms possess both α and β spins. Now, the spin arrangements, but clearly not the densities, in the vacancy quintet and singlet states are similar to those in the quartet and doublet states in the Li defect, so that all strong peaks in the Raman not seen in the vacancy spectra, can, unequivocally, be attributed to vibrational modes involving the Li atom. Figure 3 compares the predicted Raman spectra of $(C_{63}Li)_{1/2}$ and $(C_{63}Li)_{3/2}$ supercells with those of $(C_{63}V)_0$ and $(C_{63}V)_2$, from which two general points emerge. The first is that the presence of the Li atom completely destroys the vibrational mode in the host which gives rise to the 1318 cm^{-1} line, whereas it is retained in the vacancy spectra; and second, that there are clear and evident differences between the spectra of the two Li spin states across the entire spectral range, principally the regions 190 cm^{-1} to 420 cm^{-1}, and 800 cm^{-1} to 1200 cm $^{-1}$. Starting with the first of these two regions, the lowest intense peaks in the spin 3/2 state occur at 186 cm^{-1} and 194 cm^{-1}, where the first is of A_1 symmetry and the second of E symmetry, while the spin 1/2 peaks occur at 219 cm^{-1} and 220 cm^{-1}, and are of A′ and B″ symmetry respectively. In both cases, the corresponding vacancy states are Raman null in this region. What is of particular interest here is that the two E modes of the quadruplet state have counterparts in the doublet state in this region of the spectrum, whereas the A_1 is apparently red shifted to 418 cm^{-1}, which is close (4%) to the 437 cm $^{-1}$ mode in the vacancy singlet state.

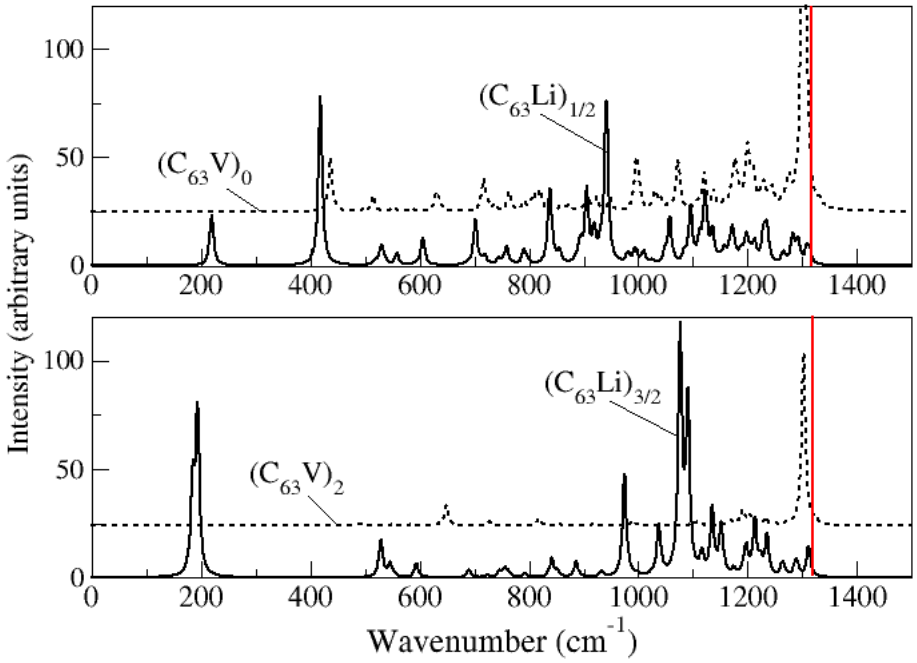

Figure 3

Comparison of the Raman spectra of $(C_{63}Li)_{1/2}$ and $(C_{63}Li)_{3/2}$ with $(C_{63}V)_0$ and $(C_{63}V)_2$. The 1318 cm $^{-1}$ ($\nu_{TO(X)}$) diamond line is shown in red.

The different symmetries, (A_1/E) and (A′/ B″), reflect the different spin distributions in the immediate vicinity of the defect site in $(C_{63}Li)_{3/2}$ and $(C_{63}Li)_{1/2}$. Now, computer animations based on normal mode analyses indicate that the A_1 186 cm^{-1} mode and doubly-degenerate E mode at 194 cm^{-1} in the spin 3/2 spectrum involve (local) symmetric and asymmetric Li-C stretch vibrations respectively, where the symmetry (and asymmetry) is determined by the motion of the three C atoms vicinal to Li with respect to the C_3-axis along the Li-C direction. Similarly, the B″ modes at 219 cm^{-1} and 220 cm^{-1} and the A′ mode at 418 cm $^{-1}$ in the spin 1/2 spectrum involve similar symmetric and asymmetric Li-C stretches. Thus, a change in the total spin of the Li defect in diamond from 3/2 to 1/2, red shifts the 194 cm^{-1} mode by ~26 cm^{-1} (13%), while the 186 cm^{-1} mode exhibits an apparent shift of 222 cm^{-1} (126%) to 418 cm^{-1}.

Above ~600 cm^{-1}, the vibrational modes are essentially collective, for both spin states, but with clear differences between them in two major respects. In the spin-3/2 spectrum, modes with intensities of ~ 1/3rd, or more, of that of the local high frequency peaks at ~200 cm $^{-1}$, occur in a region of ~250 cm^{-1}, between 970 cm^{-1} and 1220 cm^{-1}, while the intensity of the strongest peak at 1076 cm^{-1} is 1/3 *greater* than that of the local modes; in the spin-1/2 spectrum, on the other hand, there are several modes across ~500 cm^{-1} with intensities comparable to the 220 cm^{-1} modes, and none with the intensity of the local mode at 418 cm^{-1}. A possible explanation for this difference is that the rich spectrum of the vacancy singlet state in the region above 600 cm^{-1} plays a major role in determining the Li spin-1/2 spectrum, such that aside from the modes at 837 cm^{-1}, 906 cm^{-1} and 942 cm^{-1}, the remaining modes are essentially perturbations of the vacancy modes. This does not occur in the case of the Li spin-3/2 spectrum, for, as the lower panel of Figure 3

shows, the vacancy quintet spectrum is extremely sparse in this region, and hence, of little effect on that of the corresponding Li defect. What computer animations indicate is that for both spin states, these modes all involve Li-C stretches (on-bond), of exactly the same type found for the lower frequency modes, but coupled to the collective motion to a greater or lesser degree. Thus, within the entire spectral ranges of both spin states, all (Raman) peaks correspond to Li vibrations of the type indicated as (a) in Figure 4, but no off-bond vibrations of the type shown in (b).

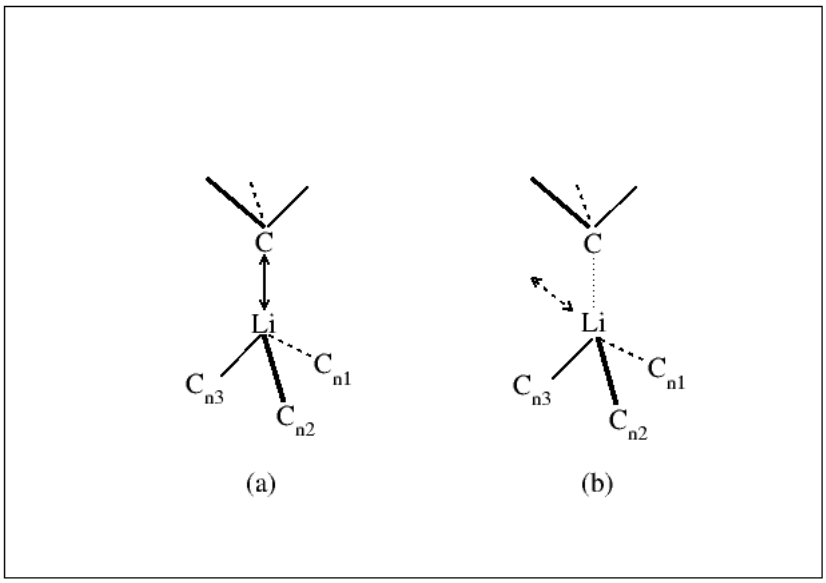

Figure 4.

Raman vibrational modes involving Li. (a) on-(Li-C)-axial stretching; (b) off-(Li-C) axial bending.

It is clear that there are manifold differences, both in frequency and intensity, between the two spin states, which can most reasonably be attributed to strong spin-phonon interactions, for the lattice relaxations in the vicinity of the Li atom are similar in the two spin states, as shown in Table II, while the atomic charges on Li and C_n also very similar, as shown in Table III.

Conclusions

In summary, the magnitudes of the frequency shifts and differences in intensity reported here are an order of magnitude greater than those reported previously for transition metal and rare-earth systems,[15-20] , with the notable exception of a very recent paper by Webster *et al*[21] on the differences in the calculated Raman spectra of the FM and AFM states of 2-dimensional CrI_3. The proximity of the charges on the four nn C atoms and their lattice relaxations, in the two spin states of the Li substitutional defect, are convincing indicators that the differences in the Raman spectra are the result of strong spin-phonon coupling. Given the relatively modest

difference in energy between the two spins states (1045 K), both spectra should be accessible experimentally.

As a final point, we comment on the stability of the present results to a change of hybrid functional, as pure DFT, like LDA and PBE, would annihilate most, if not all, the differences between the two spin states, which are the focus of this study. In the Supplementary Material the effects of varying the exact exchange percentage on the total energy and on the IR spectrum are documented. As expected, there are quantitative differences when changing from B3LYP to PBE0. Nevertheless, the qualitative results that are, in our opinion, the crucial points of this study, remain unaltered, and all the above conclusions valid.

[1] J.P. Bade, S.R. Sahaida, B.R. Stoner, J.A. Von Windheim, J.T. Glass, K. Miyata, K. Nishimura and K. Kobashi, *Fabrication of Diamond Thin-Film Thermistors for High-Temperature, Applications*. *Diam. Relat. Mater*., 1993, **2**, 816.

[2] P. Bergonzo, D. Tromson and C. Mer, *CVD Diamond-Based Semi-Transparent Beam-Position Monitors for Synchroton Beamlines: Preliminary Studies and Device Developments at CEA/Saclay*, *J. Synchroton Radiat*., 2006, **13**, 151.

[3] A. Gali, *Theory of the Neutral Nitrogen-Vacancy Centre in Diamond and its Application to the Realisation of a Qubit*, *Phys. Rev. B*, 2009, **79**, 235210.

[4] T. Schröder, M.E. Trusheim, M. Walsh, L. Li, J. Zheng, M. Schukraft, A. Sipahigil, R.E. Evans, D.D. Sukachev and C.T. Nguyen *et al.*, *Scalable Focused Ion Beam Creation of Nearly Life-Time Limited Single Quantum Emitters in Diamond Nanostructures*, *Nature Communications*, 2017, **8**, 1.

[5] C.A. Coulson, and M.J. Kearsley, *Colour Centres in Irradiated Diamonds. I, Proc. R. Soc. A*. 1957, **241**, 433.

[6] G. Davies, S.C. Lawson, A.T. Collins. A. Mainwood and S.J. Sharp, *Vacancy-Related Centers in Diamond*, *Phys. Rev. B*, 1992, **46**, 13157.

[7] S.J. Breuer and P.R. Briddon, *Ab Initio Investigation of the Native Defects in Diamond and Self-Diffusion Phys. Rev. B*, 1995, **51**, 6984.

[8] D. Hyde-Volpe, B. Slepetz, and M. Kertesz, *The {[V-C=C-V]} Divacancy and the Interstitial Defect in Diamond: Vibrational Properties*, *J. Phys. Chem.* 2010, **114**, 9563.

[9] J.P. Goss, P.R. Briddon, V. Hill, R. Jones and M.J. Rayson . *Identification of the Structure of the 3107 cm^{-1} H-Related Defect in Diamond*, *J Phys Condens Matter*. 2014, **26**, 145801.

[10] F. S. Gentile, S. Salustro, G. Di Palma, M. Causá, P. D'arco and R. Dovesi, *Hydrogen, Boron and Nitrogen Atoms in Diamond: a Quantum Mechanical Vibrational Analysis*, *Theoretical Chemistry Accounts*, **137**, 154 (2018).

[11] J.P. Goss and P.R.Briddon, *Theoretical study of Li and Na as n-type dopants for diamond*, *Phys. Rev. B*, 2007, **75**, 075202 (2007),

[12] E.B. Lombardi, A. Mainwood and K. Osuch, *Ab initio study of lithium and sodium in diamond*, *Phys. Rev. B*, 2007, **76**, 155203.

[13] H. Yilmaz, B.R. Weiner and G. Morell, *Formation of lithium clusters and their effects on conductivity in diamond: A density functional theory study*, *Diam. Relat. Mater.*, 2007, **16**, 840.

[14] J. Li, H. Yin, N. Gao, M. Zhang, J. Mu, L. Gao and H. Li, *First-principles calculations for Li, P dopants and vacancy defect in ultra-thin hydrogenated diamond nanofilms: Structural, electronic and optical properties*, *Diam. Relat. Mater*., 2019, **99**, 107526.

[15] A. Gozar, B.S .Dennis, H. Kageyama and G. Blumberg, *Symmetry and Light Coupling to Phononic and Collective Magnetic Excitations in $SrCu_2(BO_3)_2$*, *Phys.Rev. B*, 2005, **72**, 064405.

[16] D. Fausti, A.A. Nugroho, P.H.M. van Loosdrecht, S.A. Klimin, M.N. Popova and L.N. Bezmaternykh, *Raman Scattering from Phonons and Magnons in $RFe_3(BO_3)_4$*, *Phys. Rev. B*, 2006, **74**, 024403.

[17] M.O. Ramirez (+ 22 others), *Spin-Charge-Lattice Coupling Through Resonant Multimagnon Excitations in Multiferroic $BiFeO_3$*, *Appl. Phys. Lett.*, 2009, **94** 161905.

[18] F. Ziegler, H. Gibhardt, J. Leist and G. Exkold, *High-Resolution Polarised Raman Scattering Study on Spin-Phonon Soupling in Multiferroic $MnWO_4$*, *Mater. Res. Express*, 2015, **2,** 096103.

[19] A.S. Krylov, S.N. Sofronova, I.A. Gudim, S.N. Krylova, R. Kumar and A.N. Vtyurin, *Manifestation of Magnetoelastic Interactions in Raman Spectra of $Ho_xNd_{1-x}Fe_3(BO_3)_4$ Crystals*, *J. Adv. Dielec.*. 2018, **8**, 1850011.

[20] K.R. O'Neal (+13 others), *Spin-Lattice and Electron-Phonon Coupling in 3d/5d hybrid Sr_3NiIrO_6*, *NPJ Quantum Materials*, 2019, **4** 48.

[21] L. Webster, L. Liang and J-A. Yan, *Distinct Spin-Lattice and Spin-Phonon Interactions in Monolayer Magnetic CrI_3*, *Phys. Chem., Chem. Phys*, 2018, **20,** 2346.

[22] R. Dovesi, V.R. Saunders, C. Roetti, R. Orlando, C.M. Zicovich-Wilson, F. Pascale, B. Civalleri, K. Doll, N.M. Harrison, I.J. Bush, P. D'Arco and M. Llunell, *CRYSTAL 2017 User's Manual*, University of Torino, Torino, 2018

[23] A.D. Becke. *Density-Functional Thermochemistry. III. The Role of Exact Exchange*, *J. Chem. Phys.*, 1993, **98**, 5648.

[24] C. Lee, W. Yang, and R. Parr., *Development of the Colle-Salvetti Correlation-Energy Formula Into a Functional of the Electron Density*, *Phys. Rev. B*, 1988, **37,** 785.

[25] R. Dovesi, R. Orlando, A. Erba, C. M. Zicovich-Wilson, B. Civalleri, S. Casassa, L. Maschio, M. Ferrabone, M. D. L. Pierre, P. D'Arco, et al., *CRYSTAL14: A Program for the Ab Initio Investigation of Crystalline Solids, Int. J. Quantum Chem.*, 2014, **114**, 1287.
[26] M. M. Francl, W. J. Pietro, W. J. Hehre, J. S. Binkley, M. S. Gordon, D. J. DeFrees, and J. A. Pople, *Self-Consistent Molecular Orbital Methods. XXIII. A Polarization-Type Basis Set for Second-Row Elements, J. Chem. Phys.*, 1982, **77**, 3654.
[27] M. F. Peintinger, D. V. Oliveira and T. Bredow, *Consistent Gaussian basis sets of triple-zeta valence with polarization quality for solid-state calculations*, Journal of Computational Chemistry, 2013, **34**, 451.
[28] A.D. Becke, *A Multicenter Numerical Integration Scheme for Polyatomic Molecules, J. Chem. Phys.*, 1988, **88**, 2547.
[29] H.J. Monkhorst and J.D. Pack., *Special Points for Brillouin-Zone Integrations, Phys. Rev. B*, 1976, **13**, 5188.
[30] A.M. Ferrari, S. Salustro, F.S. Gentile, W.C. Mackrodt and R. Dovesi , *Substitutional Nitrogen in Diamond: A Quantum Mechanical Investigation of the Electronic and Spectroscopic Properties*, *Carbon*, 2018, **134**, 354.
[31] F. S. Gentile, S. Salustro, M. Causà, A. Erba, P. Carbonniére, and R. Dovesi, *The VN_3H Defect in Diamond: a Quantum-Mechanical Characterization, Phys. Chem. Chem. Phys.*, 2017, **19**, 22221.
[32] F. S. Gentile, S. Salustro, J. K. Desmarais, A. M. Ferrari, P. D'Arco and R. Dovesi, *Vibrational Spectroscopy of Hydrogens in Diamond: a Quantum Mechanical Treatment*, *Phys. Chem. Chem. Phys.*, 2018, **20**, 11930.
[33] www.ioffe.ru/SVA/NSM/Semicond/Diamond/basic.html
[34] H.J. McSkimin and P. Andreatch, *Elastic Moduli of Diamond as a Function of Pressure and Temperature*, *J. Appl. Phys.*, 1972, **43**, 2944.
[35] S. Bhagavantam and D.A.A.S. Narayana Rao, *Dielectric Constant of Diamond*, *Nature*, 1948, **171**, 729.
[36] S.A .Solin and A.K. Ramdas, *Raman Spectrum of Diamond*, *Phys. Rev. B*, 1970, **1** 1687.
[37] A. Bosak and M. Krisch, *Phonon density of states probed by inelastic x-ray scattering*, *Phys. Rev. B*, 2005, **72**, 224305.